

Paleoceanography and Paleoclimatology

RESEARCH ARTICLE

10.1029/2020PA003935

Special Section:

The Miocene: The Future of the Past

Key Points:

- We present the first continuous alkenone-based estimate of high latitude northern hemisphere sea surface temperatures from ~8.5 to 22 Myr
- Temperatures range 11°C to 20°C higher than modern mean annual temperature, with a maximum during the mid-Miocene Climatic Optimum (MCO)
- These results establish that the MCO warming and partial deglaciation of the Antarctic was part of a global climatic warming

Supporting Information:

- · Supporting Information S1
- · Data Set S1

Correspondence to:

T. D. Herbert, timothy_herbert@brown.edu

Citation:

Herbert, T. D., Rose, R., Dybkjær, K., Rasmussen, E. S., & Śliwińska, K. K. (2020). Bihemispheric warming in the Miocene Climatic Optimum as seen from the Danish North Sea. *Paleoceanography and Paleoclimatology*, *35*, e2020PA003935. https://doi.org/10.1029/2020PA003935

Received 15 MAY 2020 Accepted 6 AUG 2020 Accepted article online 26 AUG 2020

©2020. American Geophysical Union. All Rights Reserved.

Bihemispheric Warming in the Miocene Climatic Optimum as Seen From the Danish North Sea

Timothy D. Herbert¹, Rebecca Rose¹, Karen Dybkjær², Erik S. Rasmussen², and Kasia K. Śliwińska²

¹Department of Earth, Environmental and Planetary Sciences, Brown University, Providence, RI, USA, ²Geological Survey of Denmark and Greenland, Copenhagen, Denmark

Abstract The Miocene epoch witnessed major changes in climate. The marine oxygen isotope record, our best single continuous representation of the time interval, contains large shifts indicating substantial changes in the glaciation of Antarctica and/or deep ocean temperatures, with the interval of the most depleted isotopic composition occurring between ~18 and 13.9 Ma (mid-Miocene Climatic Optimum [MCO]). We present here a record of alkenone unsaturation estimates from a borehole penetrating marine sediments spanning most of the Miocene at ~56°N. Marine temperatures reconstructed for the Miocene are up to 20°C warmer than present day. A maximum occurs at the time of the MCO. The record is strikingly similar to discontinuous alkenone results published from other North Atlantic sites. As in the southern hemisphere, ocean temperature gradients were extraordinarily low in the North Atlantic in comparison to today. Our findings suggest that the MCO was a global temperature maximum and link the partial deglaciation of the Antarctic and subsequent "refrigeration" to a global forcing process. However, the small magnitude of the ocean cooling from ~14 to 10 Ma suggests a highly nonlinear (threshold) relationship between East Antarctic ice volume and global temperature.

1. Introduction

The mid-Miocene Climatic Optimum (MCO) represents a fascinating reversal in the Neogene climatic progression from an earlier Greenhouse world to the Pleistocene Icehouse (Zachos et al., 2001). The marine benthic δ^{18} O record records an interval from ~17 to ~13.91 Ma where deep ocean temperatures warmed and the Antarctic lost most of its ice volume (Holbourn et al., 2005, 2015; Miller et al., 2017; Zachos et al., 2001). During this time, relatively warm ocean waters bathed the Antarctic margin (Levy et al., 2016; Sangiorgi et al., 2018; Warny et al., 2009). Tundra fauna and flora on that continent were finally extinguished at ~13.9 Ma (Lewis et al., 2008), a timing consistent with interpreting the inflection in the benthic isotope curve as a re-refrigeration of the South Polar region (Zachos et al., 2001). For nearly 11 Myr, the Antarctic would then remain the unique location of a persistent polar ice cap.

While a focus on the Miocene glacial history of Antarctica is well warranted, it lacks the context of both global changes in temperature and on the temperature evolution of the northern high latitudes. Glaciological models coupled to general circulation climate models suggest that the Antarctic can glaciate at a much higher temperature threshold than its counterparts in the northern hemisphere (DeConto et al., 2008). This hypothesis should be testable with the acquisition of high quality paleotemperature measurements distributed globally. These remain in short supply and therefore hinder quantitative assessments of the climate forcing needed to explain the MCO and then its demise. For example, You et al. (2009) derived a global warming of 3–6°C from an assemblage of paleo-sea surface temperature (SST) estimates that heavily relied on oxygen isotopic values of foraminifera.

Over the past few years, alkenone paleothermometry has provided a new and less ambiguous picture of the evolution of SST since the mid-Miocene. Alkenone-derived global SST following the MCO declined steeply, with the most rapid pace of cooling coming between 8 and 5.4 Ma (Herbert et al., 2016). That paper and subsequent work by Super et al. (2018) that used both alkenones and GDGTs to make SST estimates encountered a significant limitation in using the alkenone paleothermometer to extend temperature estimates into the middle Miocene: by early Tortonian time (e.g., 11 Ma), alkenone values were close to or at

HERBERT ET AL. 1 of 10

saturation in most ocean study sites. Evidently, Miocene temperatures even after the MCO were warmer than previously thought.

Here we report new data derived from a high latitude sediment core (Sdr. Vium borehole is $55^{\circ}9'04.02''$ N, $8^{\circ}24'46.52''E$) that penetrates most of the Miocene marine succession, from the upper Aquitanian to the Tortonian (Dybkjær & Piasecki, 2010; Larsson et al., 2010; Rasmussen et al., 2010). Because we were able to recover alkenones from nearly all of the fine-grained facies of the borehole and because the Uk $'_{37}$ values with one exception stay in the range where the $C_{37:3}$ ketone is analytically well resolved, we provide one of the first continuous records of SST in a high latitude northern hemisphere location that captures conditions prior to and through the MCO, from what is generally regarded as one of the most reliable marine paleotemperature proxies. Our results clearly define a local maximum in SST corresponding to the MCO and demonstrate first-order synchrony between mid-Miocene warming and deglaciation in the southern hemisphere and warming in the high latitude northern hemisphere.

2. Geological Setting

During the late Oligocene the North Sea Basin evolved into a silled basin with the only connection to the ocean situated between the Shetland Platform and Fenno-Scandian Shield in the northern part of the basin (Anell et al., 2012; Eidvin et al., 2014; Rasmussen et al., 2010; Ziegler, 1990). Former connections to the Tethys and Central Atlantic oceans were closed due to compressional tectonics associated with the Alpine Orogeny and dynamic topographic uplift within the Central European Volcanic Province (Mayer et al., 2013, and references therein). The Miocene North Sea was thus bounded by the British Isle toward the west, a relatively low relief Central European landscape in the south, and the Fennoscandian Shield toward the east and north. Consequently, the current circulation pattern changed from open system with connections between major oceans to a simple counter counter-clockwise gyre with inflow from the north. During the early Miocene, strong uplift of the Shetland Platform and the western part of the Fennoscandian Shield resulted in marked influx of siliciclastic sediments which resulted in the formation of an east-ward prograding delta system off the Shetland Platform in the northern part of the North Sea and a southward prograding delta system in the eastern North Sea. The southern fringe of the basin was characterized by a paralic depositional setting with significant coal formation, especially associated with rift systems, for example, Rhine Graben and major structural features as the Sorgenfrei-Tornquist Zone (Schäfer et al., 2005).

For much of the Miocene, the southern margin of the North Sea basin saw large deltaic outbuilding as a result of the closure of the marine foreland basin in front of the Oligocene-early Miocene Alpine deformation front (Kuhlmann, 2007) and significant uplift of the Jura mountains and the formation of the Carpathian Mountains (Kuhlmann, 2007; Oszczypko, 2006). The paralic depositional that dominated the southern North Sea in the early Miocene changed during the late Miocene to fluvial system, partly braided systems (Schäfer et al., 2005). Consequently, a huge delta system, the so-called Eridanos Delta filled the southern North Sea Basin during the late Miocene. The progradation of delta systems from both the north and the southeast and south resulted in a high rate of sedimentation of the North Sea Basin during much of the Miocene (Rasmussen et al., 2010).

After an initial marine flooding in the earliest Miocene, the lower Miocene interval cored by the Sdr. Vium borehole reflects the influence of these prograding delta systems. The sediment is dominated by mud alternating with thin silt and fine-grained sand beds. The thicker sand-rich beds are normally graded and show hummocky cross-stratification and in the upper part double clay layers (see Figures 42–45 in Rasmussen et al., 2010). The late Langhian through early Tortonian saw the area flooded by fully marine clays of the Hodde, Ørnhøj, and Gram Formations (Larsson et al., 2010). This flooding was partly a result of an eustatic sea-level rise (mid-Miocene Climatic Optimum; Zachos et al., 2001) and partly associated with a tectonic reorganization in the NE European realm (Rasmussen, 2004; Rasmussen & Dybkjær, 2014; Ziegler, 1990). The drowning of the margins resulted in a sediment-starved North Sea that lasted most of the middle Miocene (Rasmussen & Dybkjær, 2014). The Gram Formation is truncated in the borehole by Pleistocene erosional surface that removes ~500 m of upper Miocene through middle Pliocene deposits. We estimate the youngest age of material sampled here at ~8.6 Ma.

The present biostratigraphic subdivision is based on dinoflagellate cyst (dinocyst) stratigraphy. As a part of a comprehensive program initiated in 1999, the dinocyst stratigraphy of more than 50 onshore boreholes and

HERBERT ET AL. 2 of 10



Figure 1. Paleogeographic map of the North Atlantic and North Sea circa 19.5 Ma, adapted from Scotese (2014) and http:scotese.com PAELOMAP PROJECT "breakup of Pangea." Locations of cores with Miocene alkenone-based SST discussed in text indicated by large stars: DSDP 608 (42°50'N, 23°05'W), ODP 907 (69°14°59'N), ODP 982 (51°31'N, 15°52'W), IODP 1404 (40°0.80'N, 51°48.60'W), and Sdr. Vdium core (55°49'N 8°24'E).

25 outcrop localities from Jylland (western part of Denmark) and, in addition, a handful of offshore wells were established (Dybkjær & Piasecki, 2010; Rasmussen et al., 2010). The suggested absolute ages of the boundaries of the 19 dinocyst zones are based on a combination of Sr-isotope dating of mollusk shells, calcareous foraminifera and Bolboforma from Danish boreholes and outcrops, and correlation with dinocyst events (first and last occurrences) in sites in the North Atlantic area and in northern Europe, dated based on Sr-isotopes, magnetostratigraphy, and foraminifera- and nannofossil stratigraphy (Dybkjær & Piasecki, 2010). A later study comparing the dinocyst stratigraphy with Sr-isotope dating of the Danish Miocene succession strongly supported the estimated ages of the dinocyst zones in the Lower Miocene and lower Middle Miocene, while the Sr-isotope age estimates of the upper Middle Miocene and Upper Miocene seem to be too old, see discussion in Eidvin et al. (2014). The Sdr. Vium research borehole is the only one of the boreholes/wells included in the study by Dybkjær and Piasecki (2010) that was cored. This borehole therefore forms the backbone of the dinocyst zonation. Of the 19 dinocyst zones defined by Dybkjær and Piasecki (2010) 10 are present in the Sdr. Vium borehole.

3. Methods

3.1. Age Model

We estimated sample ages as a function of core depth using the Bayesian age model program Bacon (Blaauw & Christen, 2011) (supporting information Table S1). Age uncertainties for each datum were estimated at 0.5 Myr—this is admittedly a crude estimate in the absence of better information. We produced two age models: one that removes thick sands from 80–89, 95–105, 159–162, and 181–185 m and one retaining original core

depth. The resulting age models (Figure 1, Table S1) suggest that rapid sedimentation characteristic of deltaic input in the Aquitanian-Burdigalian gave way to quite condensed sedimentation in the MCO, with a deposition rate of approximately 3.5 m/Myr (Figure 1). Inferred sampling resolution of the data we report varies considerably from 20 to 1,045 kyr with a median interval of 220 kyr. Clearly, orbital scale SST variability will not be resolved in the present data set.

3.2. Alkenone Analyses

A total of 47 samples were obtained for alkenone analyses and extracted with a Dionex ASE 200 system. Approximately 7 g per sample were used. Initial gas chromatographic analyses on raw extracts indicated complex matrices for many samples that interfered with reliable quantitation in the region where alkenones eluted. After experimentation with different cleanup methods, a protocol of flash column silica gel chromatography followed by silver nitrate and/or silver thiolate column cleanup (D'Andrea et al., 2007; Wang et al., 2019) yielded acceptable chromatography. For the silica gel procedure, silica gel columns in Pasteur pipettes were conditioned in 6 ml of hexane. Samples were transferred to the columns with hexane and eluted with 4 ml hexane. The alkenone fraction was eluted in 4 ml of methylene dichloride. Subsequently, samples were transferred to silver nitrate columns. The columns were flushed with 12 ml DCM and alkenones eluted with 8 ml ethyl acetate.

Gas chromatography was carried out with an Agilent 6890 GC equipped with 60 m VF-200 columns and FID detectors. Under ideal conditions, these columns allow full separation of the four C_{38} ketones (Longo et al., 2013, Figure 2). Prior to quantification, extracts were evaporated with nitrogen and reconstituted with 200 μ l of toluene spiked with n-hexatriacontane (C_{36}) and n-heptatriacontane (C_{37}) standards. Procedure entailed 1–5 μ l injections (depending on alkenone concentrations), initial temperature 90°C, increased to 255°C with 40°C/min rate, increased by 1°C/min to 300°C, increased by 10°C/min to 320°C, and an isothermal hold at 320°C for 11 min. Long-term laboratory analytical error, estimated from replicate extractions

HERBERT ET AL. 3 of 10

25724525, 2020, 10, Downloaded from https://agupubs.onlinelibrary.wiley.com/doi/10.1029/2020PA003935 by Brown University Library, Wiley Online Library on [19/12/2022]. See the Terms and Conditions (https://online

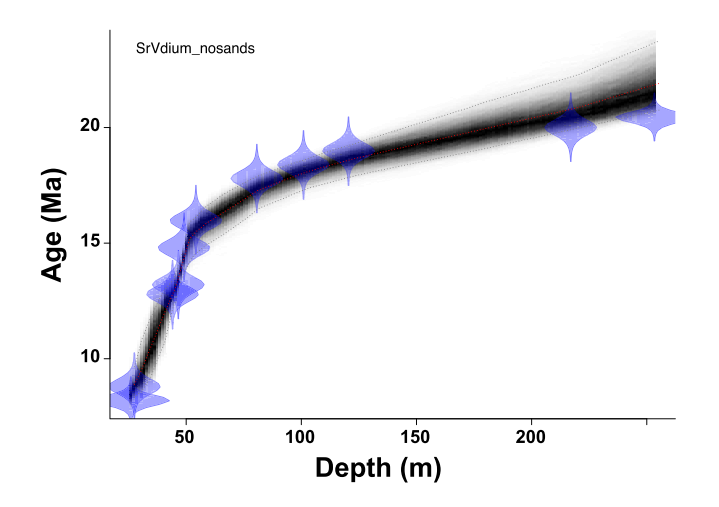


Figure 2. Age model for the Sdr. Vium core based on Bacon program (Blaauw & Christen, 2011) fit to age constraints of dinocyst biozonation (see Table S1).

and gas chromatographic analyses of a composite sediment standard, is equivalent in temperature to ± 0.1 °C and to a relative error of 10% in quantifying total C_{37} alkenones.

In all cases where we report alkenone unsaturation estimates, peaks corresponding to the $C_{37:2}$ ketone, the $C_{38:2}$ ethyl and $C_{38:2}$ methyl ketones, and the $C_{39:2}$ ethyl ketone dominate the chromatographic region where alkenones elute (examples shown in Figure 1). Four samples did not yield measurable quantities of alkenones. As an indicator of the marine source of the alkenones in a marginal environment, we calculated the sum of C_{37} to C_{38} alkenones for each sample. The average ratio was 0.88 ± 0.23 (1 sigma), consistent with a marine origin of the alkenone producers.

We report alkenone Uk'_{37} estimates of paleotemperature according to two calibrations: the widely accepted linear core top calibration of Müller et al. (1998) and the newer BAYSPLINE calibration of Tierney and Tingley (2018). While these calibrations are very similar over much of the range of Uk'_{37} , the BAYSPLINE calibration suggests curvature of the relationship at high temperatures, such that temperature estimates

become warmer than indicated by the Müller et al. (1998) calibration. As generally accepted in the alkenone literature, we reference the temperature estimates to mean annual SST (cf. Müller et al., 1998; Prahl et al., 1988; Rosell-Melé & Prahl, 2013; Tierney & Tingley, 2018), recognizing that it might be appropriate to account for some warm season production bias in this high latitude setting.

We experimented with the BAYSPLINE model, using Bayesian priors of 5 (recommended by Tierney & Tingley, 2018, for samples on the high end of Uk'₃₇ values) and 3 (which downweights temperatures above

Figure 3. Representative chromatograms (60 m VF-200 chromatographic column) of the alkenone fractions analyzed from the Sdr. Vium core following silica gel and silver nitrate column cleanups. Compound identification: A = C $_{37:3}$ methyl ketone, B = C $_{37:2}$ alkenone, C = C $_{38:3}$ ethyl ketone, D = C $_{38:2}$ ethyl ketone, E = C $_{38:3}$ methyl ketone, F = C $_{38:2}$ methyl ketone, G = C $_{39:3}$ ethyl ketone, H = C $_{39:2}$ ethyl ketone. Note that compounds C, E, and G are not always resolved well enough in the Sdr. Vium extracts to allow quantification (e.g., sample at 285.5 m).

the highest SST values for the modern ocean). We hesitate to adopt the Tierney and Tingley (2018) approach because it potentially amplifies noise (difficulty in accurately determining the very small $C_{37:3}$ peak area at high Uk'_{37}) into signal, but we report these estimates to let the reader judge the effect of calibration uncertainties (Table S2). While mean estimated values for SST derived from the Sdr. Vium core are very similar using the Müller et al. (1998, 27.09°C), Tierney and Tingley (2018, prior = 5, 27.56°C; prior = 3, 27.13°C), the ranges of the BAYSPLINE estimated temperatures (8.7°C and 7.8°C) are larger than for the Müller et al. (1998) calibration (6.5°C) due to the nonlinearity of the BAYSPLINE fit.

4. Results

Alkenone unsaturation estimates yield very high unsaturation values throughout the Miocene interval (Figure 3, Table S2). Converted to temperature, the alkenone proxy suggests strikingly warm temperatures in the Danish North Sea throughout the recovered Miocene interval. In one sample at 58.7 m (~15,500 ka), the $\rm C_{37:3}$ peak is so small as to be below confident detection limit, suggesting an unsaturation value of 1.0. Uk' $_{37}$ values stay consistently very warm (above 0.95) from 91.1 to 47.5 m (~17.1–13.8) Ma and decline on either side of the MCO. Alkenone abundances vary considerably and reach their maximum in the MCO (Figure 2, Table S2). These higher concentrations could reflect more open marine conditions that supported higher alkenone production, a decrease in clastic dilution associated with transgression, or both. In general, concentrations are on the low end for typical pelagic sediments encountered in the Brown alkenone laboratory.

HERBERT ET AL. 4 of 10

25724525, 2020, 10, Downloaded from https://agupubs.onli

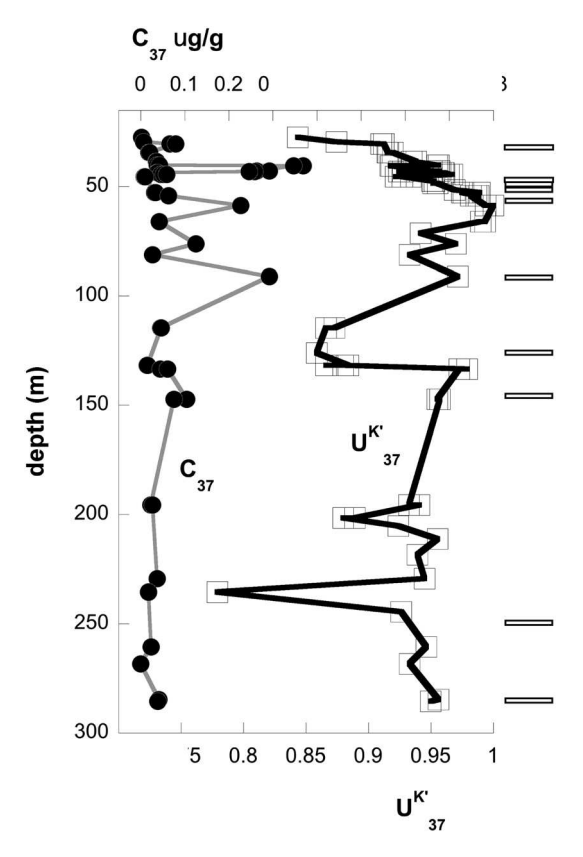


Figure 4. $U^{k'}_{37}$ and total C_{37} alkenones (C_{37} total as ug/g dry weight sediment) as a function of core depth. Position of dinocycst biostratigraphic datums (see Table S1) indicated by horizontal bars

5. Discussion

We explore here the interpretation of alkenone results from the Sdr. Vium core for regional ocean temperatures, for connections to faunal and floral evolution in northwestern Europe, and then to larger scale hemispheric and global climate patterns during the Miocene. The first question arises as to interpret the Uk'37 values obtained. Although alkenone unsaturation values are generally calibrated to mean annual SST, this model is clearly an idealization, particularly at high latitudes where production is likely to be negligible during winter months. The mean annual SST for the region is about 10°C, with an annual range from about 8°C to 18°C (https://iridl.ldeo.columbia.edu/maproom/Global/ Ocean_Temp/Monthly_Temp.html). The Sdr. Vium alkenone values thus all lie well above the warmest temperatures recorded in the eastern North Sea today. Furthermore, while evidence of a North Atlantic late summer/early fall bias has been reported in modern calibration studies (Tierney & Tingley, 2018), the offset from mean annual SST is modest (on the order of 3°C). One can also question how the generally milder climate and generally ice-free Arctic conditions of the middle Miocene (Stein et al., 2016) would affect the seasonal range of temperatures—it seems likely that North Sea winter SST would be closer to mean annual temperature than today without the cooling induced by Arctic sea ice and also winter snow cover on land. We therefore suggest that the alkenone-based SST estimates approximate mean annual temperatures.

Comparison to biomarker-based Miocene reconstructions from the North Atlantic also aids in judging how representative our new record is (Figure 4). It is clear that the trends and magnitude of Miocene warmth here fit very well. The Sdr. Vium record is unique in that it continuously records SST before, during, and after the MCO. The record at DSDP 608 (latitude of 42°50′N) becomes saturated with respect to Uk′₃₇ in the

MCO interval (Super et al., 2018), while sites to the North (ODP 982, 907 and Sdr.Vium) stay below the 1.0 threshold, as would be expected from their higher latitude locations. Temperatures recorded in the Danish North Sea are nearly identical to those reported from ODP 982 (Herbert et al., 2016), despite the fact that the modern seasonal temperature range at Site 982 is only 5°C—a further indication that our new data do not suffer from a strong seasonal bias.

What is common to all North Atlantic SST records is a local maximum in amplitude from ~14–17 Ma, accompanied by very small latitudinal gradients in temperature. Notably, temperatures before and after the MCO remained much higher than today for extended periods of time: The bulk of North Atlantic cooling occurred only after ~8 Ma (Herbert et al., 2016). The paleogeography of the Miocene North Sea made it a window into the Arctic (Rasmussen et al., 2008). While we cannot extrapolate North Sea SST to the Arctic, the warmth we reconstruct is consistent with low resolution SST estimates from the Arctic for ice free summers in windows from ~6.5–7 Ma and 8–11.5 Ma (Stein et al., 2016). How well do the new SST estimates of Super et al. (2018) and this work fit a previous reconstruction of marine temperature anomalies at 10 Ma? As Figure 6 demonstrates, the new data are surprisingly consistent and solidify a previous estimate of mean global SST warming on the order of 6°C (relative to present day) at 10 Ma (Herbert et al., 2016).

The marine temperatures we infer are qualitatively consistent with faunal and floral reconstructions of a warm and wet northwestern Europe for most of the Miocene (Böhme, 2003; Fortelius et al., 2014; Grímsson et al., 2007; Larsson et al., 2011; Mörs, 2002; Mosbrugger et al., 2005; Pound et al., 2011, 2012; Utescher et al., 2011, 2017). Larsson et al. (2011) studied pollen assemblages from 160 to 25 m of the Sdr. Vium core. The assemblage was overwhelmingly dominated by gymnosperms. Two paleoecological groupings explained most of the variance: swamp-forest taxa and deciduous-evergreen mixed forest (up to 75% and 50% of assemblages, respectively). Their reconstruction has deciduous-evergreen mixed forests bordering swamp forests with a high fraction of the deciduous component (evergreens were mostly small

HERBERT ET AL. 5 of 10

25724525, 2020, 10, Downloaded from https://agupubs.onlinelibrary.wiley.com/doi/10.1029/2020PA003935 by Brown University Library, Wiley Online Library on [19/12/2022]. See the Terms and Conditions (https://onlinelibrary.wiley.com/

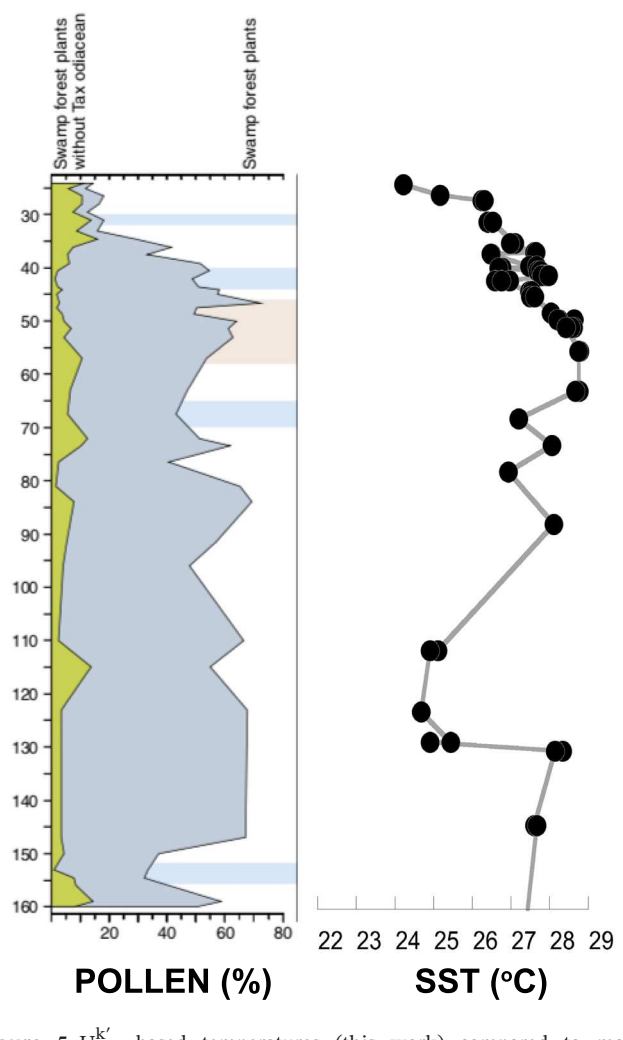


Figure 5. $U^{k'}_{37}$ -based temperatures (this work) compared to major vegetation changes reconstructed for the middle-late Miocene in the Sdr. Vium core (adapted from Larsson et al., 2011)

trees and shrubs). This reconstruction is quite similar to previous work on lower Miocene pollen assemblages from Denmark (Larsson et al., 2010). Swamp forest plants dominate to end of the Serravalian (at the approximate level of 40 m in the core) when conifer forest increases significantly (Figure 5). This shift is associated with a decline in marine temperatures to below 26°C. We observe also that as temperatures decline below 24°C, *Poaceae* (grasses) increase (at ~32 m, equivalent to ~9,800 ka) to 15% (Larsson et al., 2011)

Miocene pollen and spore assemblages in north western Europe have been translated to temperature estimates by a number of approaches (Larsson et al., 2011; Utescher et al., 2009). Most directly relevant to the present study is a coexistence approach to estimate temperatures from the pollen assemblage in the Sdr. Vium core (Larsson et al., 2011). This study yielded an estimate of 15.5–20°C for mean annual temperature (MAT, 8.5–12.5°C for the coldest mean month [CMM] and 23–27°C for the warmest mean month [WMM]). Slightly south from our study location, Utescher et al. (2009, 2011, 2017) have produced similar estimates from the Rhine Basin. They reconstruct a continental temperature maximum in the MCO, peaking at ~18°C MAT, although they also note that there is no modern equivalent to the MCO flora (Utescher et al., 2009). Seasonality and the number of frost days increased markedly in the late Miocene (Utescher et al., 2009).

On a broader scale, Utescher et al.'s (2017) survey of MAT and CMM from floras over a latitude range of 15–65° North in North America and Europe/Western Eurasia documents very gentle temperature gradients as inferred from vegetation analysis. At the latitude of the Sdr. Vium core, their reconstruction indicates a MAT of ~18°C (but up to 22°C including variance) and temperatures well above freezing to 70°N. The CMM estimate produces even bigger anomalies relative to the present (warmer by ~8°C at the latitude of Denmark), and only crosses the freezing point at ~65°N.

In the vertebrate realm, the alligator *Diplocynodon* was common in the Hambach C level (equivalent to the MCO) of the Rhine Basin as were rhinoceri adapted to a semiaquatic mode of living (Mörs, 2002). Böhme (2003) reports two main migration events of thermophilic ectotherms at 20 and 18 Ma that indicate the beginning of the Miocene Climatic Optimum in Central Europe (42–45°N palaeolatitude).

According to this study, the minimum MAT would have been 17.4°C, with a preferred estimate of 20–24°C. Furthermore, "The warm period ended abruptly between 14.0 and 13.5 Ma (Middle/Late Badenian transition) with major regional extinction events of most of the thermophilic groups in Central Europe and a drop of the MAT of probably more than 7°C to temperatures around 14.8–15.7°C. This drop can be attributed predominantly to a decrease of more than 11°C of the minimum cold months temperature. This temperature decrease marked the beginning of a climatic zonation of the European continent and is also evidenced by a progressively southward disappearance of the crocodile *Diplocynodon* from 38–45°N palaeolatitude to 30–37°N during the Middle and earliest Late Miocene" (Böhme, 2003).

Our marine SST reconstruction provides a boundary condition for estimating temperatures in northwestern Europe and suggests that terrestrial temperature estimates for the Miocene cited above, while qualitatively consistent with the new data, are most likely conservative. Indeed, it seems likely that improvements in spatial coverage of SST estimates, in conjunction with climate models, can be used to better infer the temperature ranges experienced by fauna and flora in the late Miocene (cf. Henrot et al., 2017).

The warm Miocene climate over northwestern Europe was also apparently significantly wetter than present (Bruch et al., 2011). Larsson et al. (2011) report pollen-based estimates of mean annual precipitation of

HERBERT ET AL. 6 of 10

25724525, 2020, 10, Downloaded from https://agupubs.onlinelibrary.wiley.com/doi/10.1029/2020PA003935 by Brown University Library, Wiley Online Library on [19/12/2022]. See the Terms and Conditions (https://onlinelibrary.wiley.com/erms

and-conditions) on Wiley Online Library for rules of use; OA articles are governed by the applicable Creative Commons License

Difference SST 10Ma-present Global SST anomaly = +6.2°C Global SST anomaly = +6.2°C 70 70 South North

Figure 6. Compilation of biomarker-based SST (Tierney & Tingley, 2018, calibration) in the North Atlantic from Miocene to present. IODP 1404 at 40°N, 51.60 W (Liu et al., 2018); Site 608 is from 42°50 N, 23°05 W (Super et al., 2018), 982 is located at 51°31 N, 15°52 W (Herbert et al., 2016), 907 is at 69°14.989′N, 12°41.894′E (Herbert et al., 2016), DM is Sdr. Vium core (this paper).

Latitude, area weighted

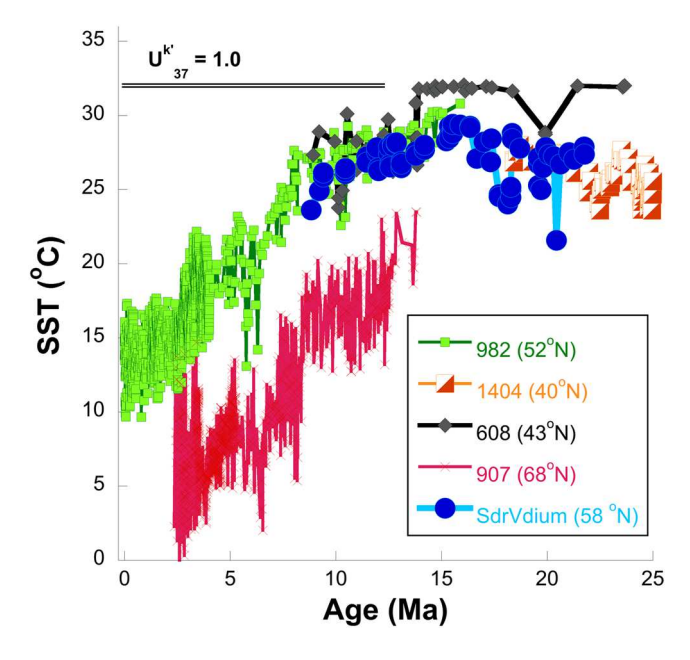


Figure 7. Alkenone-based SST anomaly (relative to present day) at 10 Ma, taken from Herbert et al. (2016) with new points from DSDP 608 (Super et al., 2018) and Sdr. Vium core (this work) shown as larger squares. The integrated global ocean surface anomaly is ~6°C, corresponding to a mean air surface anomaly of ~10°C.

1,200–1,750 mm from the Sdr. Vium core versus ~600 mm today. The authors do not find any notable trends in precipitation over time. A warm, wet climate in the region is also indicated by coal-bearing prograding deltaic units of the Odderup Formation (first half of the Langhian) in the Danish North Sea region (Rasmussen et al., 2010) and brown coals of the Rhine Basin, which range from lower through middle Miocene in age (Utescher et al., 2012). Indeed, Fortelius et al. (2014) reconstruct the time period 23–15 Ma as wet over nearly all Europe, with N-S gradients developing in late Miocene along with an expansion of arid areas.

These temperature, faunal, and floral trends in the northern hemisphere appear coeval with similar changes in the high latitudes of the southern hemisphere. During the MCO, dinocyst assemblages from off the Adelie Coast (IODP Site U1356, ~63°S) testify to surface waters similar to today's subtropical front (Sangiorgi et al., 2018). Ice retreated inland at the same time, allowing for pollen from coastal vegetation to accumulate at Site U1356. TEX-based temperatures suggest SST of 11.2-16.7°C in water that is at ~0°C today; pollen assemblages and leaf wax δD reconstruct coastal temperatures between 5.8°C and 13.8°C (Feakins et al., 2012; Sangiorgi et al., 2018, Warny et al., 2009; Warny & Askin, 2011). Poleward, results of Andrill drilling reveal alternating episodes of cold polar and open ocean conditions during the MCO, with exceptionally warm intervals at ~16.4 and 15.9 Ma (Levy et al., 2016). In a similar manner to the North Atlantic data shown in Figure 5, SST gradients in the southern hemisphere were very mild (Sangiorgi et al., 2018), although the SST estimate at ODP Site 1,171 (48°30'S) based on Mg/Ca ratio in the planktonic foraminifer G. bulloides (Shevenell et al., 2004) need to be revised upward to account for the lower (and poorly constrained) Miocene Mg/Ca ratio in seawater, increasing the gradient to IODP 1356 estimated by Sangiorgi et al. (2018).

High latitude paleotemperature estimates thus unequivocally demonstrate the global nature of MCO warming and associate the warming very closely with retreat of the Antarctic ice sheet, as seen both by proxy evidence (e.g., Levy et al., 2016; Sangiorgi et al., 2018) and stable isotopic evidence (e.g., Holbourn et al., 2013, 2014; Miller et al., 2017; Shevenell et al., 2004; Zachos et al., 2001). Any mechanism to generate Miocene warmth must thus satisfy the approximately symmetrical warming revealed by marine SST profiles. How warm was the MCO? Alkenone-based estimates are hampered by saturation, although they provide a minimum estimate of warming to >29°C at the following locations in the Pacific Ocean (DSDP 588, 26°06S, 161°13.6E, Pagani et al., 1999), North Atlantic (DSDP 608, 42°50N, 23°05W, Pagani et al., 1999; Super et al., 2018), Arabian Sea (ODP 730, 17°43.885°N, 57°41.519E, Pagani et al., 1999), tropical Atlantic (ODP 925, 4°12.249'N, 43°29.334'W, Zhang et al., 2013). Tropical Pacific (IODP 1338, paleo-location of ~1.3°N, 110°W, Rousselle et al., 2013), Paratethys (48°N, 13°E, Grunert et al., 2014), and Mediterranean (35°57N, 14°18E, Badger et al., 2013). It seems safe to conclude that alkenone estimates preclude a "cool tropics" reconstruction (cf. You et al., 2009). Unfortunately, more quantitative estimation of mid-Miocene tropical temperatures depends on other proxies, a topic that has generated much controversy (Zhang et al., 2014).

A first estimate of global MCO warmth might take the alkenone-based reconstruction at 10 Ma (Figure 6) as a baseline and extrapolate to the warmer MCO. North Atlantic SST is 2–3°C warmer at the MCO at sites

HERBERT ET AL. 7 of 10

8 of 10

Acknowledgments

We gratefully acknowledge support

from National Science Foundation

(NSF) grant 1635127 to T. D. H. and

funding from Geocenter Denmark to

Naafs, and M. Huber for constructive

K. S. We thank J. E. Tierney, D. M.

comments that improved the

HERBERT ET AL.

manuscript.

where the Uk'_{37} index is not saturated (Figure 7). Pulses of warm-water mollusks in the high latitude North Pacific suggest that this was a hemisphere-wide warming (Oleinik et al., 2009). In the southern hemisphere, high resolution Mg/Ca data from ODP Site 1,171 also show that the time-averaged temperatures of the MCO were 2–3°C warmer than the following 2 Ma, although the transition to colder temperatures at ~13.9 Ma is abrupt (Shevenell et al., 2004). Close to the Antarctic, the Adelie Coast cooled but remained much warmer than today immediately after the MCO (Sangiorgi et al., 2018). In aggregate, ocean cooling following the MCO therefore appears moderate, not severe. A rough estimate of global ocean warming at the MCO of 7–9°C relative to present day seems in order- recognizing that variability within the MCO (Holbourn et al., 2005, 2007; Levy et al., 2016; Miller et al., 2017; Shevenell et al., 2004) is not resolved. This estimate is much higher than generally used as a baseline for modeling the behavior of the Antarctic ice sheet during the MCO (cf. Gasson et al., 2016).

If ocean temperatures preceding and post-dating the MCO were as warm as reconstructed here, the disappearance and regrowth of Antarctic ice volume during the mid-Miocene occurred over a modest range of global temperatures, in a generally warm state. Estimating the contribution of ice volume as opposed to deep ocean temperature change remains difficult, of course (Shevenell et al., 2008). Nevertheless, the existence of quite warm marine temperatures both preceding and immediately post-dating the MCO suggests that Antarctic glaciation was poised in a very sensitive region of climate space—a region where only a few degrees of marine temperature change corresponded to large changes in ice volume. This sensitivity perhaps accounts for the rapidity of reglaciation after ~13.91 Ma (Holbourn et al., 2005; Shevenell et al., 2004) and variable conditions in the Antarctic in the early Miocene (Griener et al., 2015).

Data Availability Statement

The data presented in this article will be available on the Pangaea repository (https://doi.pangaea.de/10.1594/PANGAEA.921249).

References

- Anell, I., Thybo, H., & Rasmussen, E. (2012). A synthesis of Cenozoic sedimentation in the North Sea. Basin Research, 24(2), 154–179. https://doi.org/10.1111/ji.1365-2117.2011.00517.x
- Badger, M. P., Lear, C. H., Pancost, R. D., Foster, G. L., Bailey, T. R., Leng, M. J., & Abels, H. A. (2013). CO₂ drawdown following the middle Miocene expansion of the Antarctic ice sheet. *Paleoceanography*, 28, 42–53. https://doi.org/10.1002/palo.20015
- Blaauw, M., & Christen, J. A. (2011). Flexible paleoclimate age-depth models using an autoregressive gamma process. *Bayesian Analysis*, 6(3), 457–474.
- Böhme, M. (2003). The Miocene climatic optimum: Evidence from ectothermic vertebrates of Central Europe. *Palaeogeography, Palaeoclimatology, Palaeoecology, 195*(3–4), 389–401. https://doi.org/10.1016/S0031-0182(03)00367-5
- Bruch, A. A., Utescher, T., Mosbrugger, V., & Members, N. (2011). Precipitation patterns in the Miocene of Central Europe and the development of continentality. *Palaeogeography, Palaeoclimatology, Palaeoecology*, 304(3–4), 202–211. https://doi.org/10.1016/j. palaeo.2010.10.002
- D'Andrea, W. J., Liu, Z., Alexandre, M. D. R., Wattley, S., Herbert, T. D., & Huang, Y. (2007). An efficient method for isolating individual long-chain alkenones for compound-specific hydrogen isotope analysis. *Analytical Chemistry*, 79(9), 3430–3435. https://doi.org/10.1021/ac062067w
- DeConto, R. M., Pollard, D., Wilson, P. A., Pälike, H., Lear, C. H., & Pagani, M. (2008). Thresholds for Cenozoic bipolar glaciation. *Nature*, 455(7213), 652–656. https://doi.org/10.1038/nature07337
- Dybkjær, K., & Piasecki, S. (2010). Neogene dinocyst zonation for the eastern North Sea Basin, Denmark. *Review of Palaeobotany and Palynology*, 161(1–2), 1–29. Retrieved from <go to ISI>://WOS:000279563300001
- Eidvin, T., Riis, F., & Rasmussen, E. S. (2014). Oligocene to lower Pliocene deposits of the Norwegian continental shelf, Norwegian Sea, Svalbard, Denmark and their relation to the uplift of Fennoscandia: A synthesis. *Marine and Petroleum Geology*, 56, 184–221. https://doi.org/10.1016/j.marpetgeo.2014.04.006
- Feakins, S. J., Warny, S., & Lee, J.-E. (2012). Hydrologic cycling over Antarctica during the middle Miocene warming. *Nature Geoscience*, 5(8), 557–560. https://doi.org/10.1038/ngeo1498
- Fortelius, M., Eronen, J. T., Kaya, F., Tang, H., Raia, P., & Puolamäki, K. (2014). Evolution of Neogene mammals in Eurasia: Environmental forcing and biotic interactions. *Annual Review of Earth and Planetary Sciences*, 42(1), 579–604. https://doi.org/10.1146/annurev-earth-050212-124030
- Gasson, E., DeConto, R. M., Pollard, D., & Levy, R. H. (2016). Dynamic Antarctic ice sheet during the early to mid-Miocene. *Proceedings of the National Academy of Sciences*, 113(13), 3459–3464. https://doi.org/10.1073/pnas.1516130113
- Griener, K. W., Warny, S., Askin, R., & Acton, G. (2015). Early to middle Miocene vegetation history of Antarctica supports eccentricity-paced warming intervals during the Antarctic icehouse phase. *Global and Planetary Change*, 127, 67–78. https://doi.org/10.1016/j.gloplacha.2015.01.006
- Grímsson, F., Denk, T., & Símonarson, L. A. (2007). Middle Miocene floras of Iceland—The early colonization of an island? Review of Palaeobotany and Palynology, 144(3-4), 181–219. https://doi.org/10.1016/j.revpalbo.2006.07.003
- Grunert, P., Tzanova, A., Harzhauser, M., & Piller, W. E. (2014). Mid-Burdigalian Paratethyan alkenone record reveals link between orbital forcing, Antarctic ice-sheet dynamics and European climate at the verge to Miocene climate optimum. *Global and Planetary Change*, 123, 36–43. https://doi.org/10.1016/j.gloplacha.2014.10.011

125, 50–45. https://doi.org/10.1010/j.gtopiacha.2014.10.011

- Henrot, A.-J., Utescher, T., Erdei, B., Dury, M., Hamon, N., Ramstein, G., et al. (2017). Middle Miocene climate and vegetation models and their validation with proxy data. *Palaeogeography, Palaeoclimatology, Palaeoecology, 467*, 95–119. https://doi.org/10.1016/j. palaeo.2016.05.026
- Herbert, T. D., Lawrence, K. T., Tzanova, A., Peterson, L. C., Caballero-Gill, R., & Kelly, C. S. (2016). Late Miocene global cooling and the rise of modern ecosystems. *Nature Geoscience*, 9(11), 843–847. https://doi.org/10.1038/ngeo2813
- Holbourn, A., Kuhnt, W., Frank, M., & Haley, B. A. (2013). Changes in Pacific Ocean circulation following the Miocene onset of permanent Antarctic ice cover. *Earth and Planetary Science Letters*. 365, 38–50. https://doi.org/10.1016/j.epsl.2013.01.020
- Holbourn, A., Kuhnt, W., Kochhann, K. G. D., Andersen, N., & Sebastian Meier, K. J. (2015). Global perturbation of the carbon cycle at the onset of the Miocene climatic optimum. *Geology*, 43(2), 123–126. https://doi.org/10.1130/G36317.1
- Holbourn, A., Kuhnt, W., Lyle, M., Schneider, L., Romero, O., & Andersen, N. (2014). Middle Miocene climate cooling linked to intensification of eastern equatorial Pacific upwelling. Geology, 42(1), 19–22. https://doi.org/10.1130/G34890.1
- Holbourn, A., Kuhnt, W., Schulz, M., & Erlenkeuser, H. (2005). Impacts of orbital forcing and atmospheric carbon dioxide on Miocene ice-sheet expansion. *Nature*, 438(7067), 483–487. https://doi.org/10.1038/nature04123
- Holbourn, A., Kuhnt, W., Schulz, M., Flores, J.-A., & Andersen, N. (2007). Orbitally-paced climate evolution during the middle Miocene "Monterey" carbon-isotope excursion. *Earth and Planetary Science Letters*, 261(3–4), 534–550. https://doi.org/10.1016/j.epsl.2007.07.026
- Kuhlmann, J. (2007). Paleogeographic and paleotopographic evolution of the Swiss and eastern Alps since the Oligocene. *Global and Planetary Change*, 58(1–4), 224–236. https://doi.org/10.1016/j.gloplacha.2007.03.007
- Larsson, L. M., Dybkjær, K., Rasmussen, E. S., Piasecki, S., Utescher, T., & Vajda, V. (2011). Miocene climate evolution of northern Europe: A palynological investigation from Denmark. *Palaeogeography, Palaeoclimatology, Palaeoecology, 309*(3–4), 161–175. https://doi.org/10.1016/j.palaeo.2011.05.003
- Larsson, L. M., Vajda, V., & Dybkjaer, K. (2010). Vegetation and climate in the latest Oligocene-earliest Miocene in Jylland, Denmark. Review of Palaeobotany and Palynology, 159(3–4), 166–176. Retrieved from <go to ISI>://WOS:000275688400003
- Levy, R., Harwood, D., Florindo, F., Sangiorgi, F., Tripati, R., von Eynatten, H., et al. (2016). Antarctic ice sheet sensitivity to atmospheric CO₂ variations in the early to mid-Miocene. *Proceedings of the National Academy of Sciences*, 113(13), 3453–3458. https://doi.org/10.1073/pnas.1516030113
- Lewis, A. R., Marchant, D. R., Ashworth, A. C., Hedenäs, L., Hemming, S. R., Johnson, J. V., et al. (2008). Mid-Miocene cooling and the extinction of tundra in continental Antarctica. *Proceedings of the National Academy of Sciences*, 105(31), 10,676–10,680. https://doi.org/10.1073/pnas.0802501105
- Liu, Z., He, Y., Jiang, Y., Wang, H., Liu, W., Bohaty, S. M., & Wilson, P. A. (2018). Transient temperature asymmetry between hemispheres in the Palaeogene Atlantic Ocean. *Nature Geoscience*, 11(9), 656–660. https://doi.org/10.1038/s41561-018-018-09
- Longo, W. M., Dillon, J. T., Tarozo, R., Salacup, J. M., & Huang, Y. (2013). Unprecedented separation of long chain alkenones from gas chromatography with a poly (trifluoropropylmethylsiloxane) stationary phase. *Organic Geochemistry*, 65, 94–102. https://doi.org/10.1016/j.orggeochem.2013.10.011
- Mayer, B., Jung, S., Romer, R. L., Stracke, A., Haase, K., & Garbe-Schönberg, C.-D. (2013). Petrogenesis of tertiary hornblende-bearing lavas in the Rhön, Germany. *Journal of Petrology*, 54(10), 2095–2123. https://doi.org/10.1093/petrology/egt042
- Miller, K. G., Baluyot, R., Wright, J. D., Kopp, R. E., & Browning, J. V. (2017). Closing an early Miocene astronomical gap with Southern Ocean δ¹⁸O and δ¹³C records: Implications for sea level change. *Paleoceanography*, 32, 600–621. https://doi.org/10.1002/2016PA003074
- Mörs, T. (2002). Biostratigraphy and paleoecology of continental tertiary vertebrate faunas in the lower Rhine embayment (NW-Germany). Netherlands Journal of Geosciences - Geologie en Mijnbouw, 81(2), 177–183. https://doi.org/10.1017/S0016774600022411
- Mosbrugger, V., Utescher, T., & Dilcher, D. L. (2005). Cenozoic continental climatic evolution of Central Europe. *Proceedings of the National Academy of Sciences of the United States of America*, 102(42), 14,964–14,969. https://doi.org/10.1073/pnas.0505267102
- Müller, P. J., Kirst, G., Ruhland, G., von Storch, I., & Rosell-Melé, A. (1998). Calibration of the alkenone paleotemperature index U'₃₇ based on core-tops from the eastern South Atlantic and the global ocean (60°N–60°S). *Geochimica et Cosmochimica Acta*, 62(10), 1757–1772. https://doi.org/10.1016/S0016-7037(98)00097-0
- Oleinik, A., Marincovich, L. Jr., Barinov, K. B., & Swart, P. K. (2009). Magnitude of middle Miocene warming in North Pacific high latitudes: Stable isotope evidence from Kaneharaia (Bivalvia, Dosiniinae). *Bulletin of the Geological Survey of Japan*, 59(7–8), 339–353. https://doi.org/10.9795/bullgsj.59.339
- Oszczypko, N. (2006). Late Jurassic-Miocene evolution of the outer Carpathian fold-and-thrust belt and its foredeep basin (Western Carpathians, Poland). *Geological Quarterly*, 50(1), 169–194.
- Pagani, M., Arthur, M. A., & Freeman, K. H. (1999). Miocene evolution of atmospheric carbon dioxide. *Paleoceanography*, 14(3), 273–292. https://doi.org/10.1029/1999pa900006
- Pound, M. J., Haywood, A. M., Salzmann, U., & Riding, J. B. (2012). Global vegetation dynamics and latitudinal temperature gradients during the mid to late Miocene (15.97–5.33 Ma). Earth-Science Reviews. 112(1–2), 1–22. https://doi.org/10.1016/j.earscirev.2012.02.005
- Pound, M. J., Haywood, A. M., Salzmann, U., Riding, J. B., Lunt, D. J., & Hunter, S. J. (2011). A Tortonian (late Miocene, 11.61–7.25 Ma) global vegetation reconstruction. *Palaeogeography, Palaeoclimatology, Palaeoecology, 300*(1–4), 29–45. https://doi.org/10.1016/j. palaeo.2010.11.029
- Prahl, F. G., Muehlhausen, L. A., & Zahnle, D. L. (1988). Further evaluation of long-chain alkenones as indicators of paleoceanographic conditions. *Geochimica et Cosmochimica Acta*, 52(9), 2303–2310. https://doi.org/10.1016/0016-7037(88)90132-9
- Rasmussen, E., & Dybkjær, K. (2014). Patterns of Cenozoic sediment flux from western Scandinavia: Discussion. Basin Research, 26(2), 338–346. https://doi.org/10.1111/bre.12024
- Rasmussen, E. S. (2004). Stratigraphy and depositional evolution of the uppermost Oligocene–Miocene succession in western Denmark. Bulletin of the Geological Society of Denmark, 51(2), 89–109.
- Rasmussen, E. S., Dybkjær, K., & Piasecki, S. (2010). Lithostratigraphy of the upper Oligocene–Miocene succession of Denmark. *Geological Survey of Denmark and Greenland Bulletin*, 22, 92.
- Rasmussen, E. S., Heilmann-Clausen, C., Waagstein, R., & Eidvin, T. (2008). The tertiary of Norden. *Episodes*, 31(1), 66–72. https://doi.org/10.18814/epiiugs/2008/v31i1/010
- Rosell-Melé, A., & Prahl, F. G. (2013). Seasonality of UK′₃₇ temperature estimates as inferred from sediment trap data. *Quaternary Science Reviews*, 72, 128–136. https://doi.org/10.1016/j.quascirev.2013.04.017
- Rousselle, G., Beltran, C., Sicre, M.-A., Raffi, I., & De Rafelis, M. (2013). Changes in sea-surface conditions in the equatorial Pacific during the middle Miocene–Pliocene as inferred from coccolith geochemistry. *Earth and Planetary Science Letters*, 361, 412–421. https://doi.org/10.1016/j.epsl.2012.11.003

HERBERT ET AL. 9 of 10

- Sangiorgi, F., Bijl, P. K., Passchier, S., Salzmann, U., Schouten, S., McKay, R., et al. (2018). Southern Ocean warming and Wilkes land ice sheet retreat during the mid-Miocene. *Nature Communications*, 9(1), 1–11.
- Schäfer, A., Utescher, T., Klett, M., & Valdivia-Manchego, M. (2005). The Cenozoic lower Rhine Basin—Rifting, sedimentation, and cyclic stratigraphy. *International Journal of Earth Sciences*, 94(4), 621–639. https://doi.org/10.1007/s00531-005-0499-7
- Scotese, C. R. (2014). Atlas of Neogene Paleogeographic Maps (Mollweide Projection), Maps 1-7, Volume 1, The Cenozoic, PALEOMAP Atlas for ArcGIS. Evanston, IL: PALEOMAP Project. https://doi.org/10.13140/2.1.4151.3922
- Shevenell, A. E., Kennett, J. P., & Lea, D. W. (2004). Middle Miocene Southern Ocean cooling and Antarctic cryosphere expansion. *Science*, 305(5691), 1766–1770. https://doi.org/10.1126/science.1100061
- Shevenell, A. E., Kennett, J. P., & Lea, D. W. (2008). Middle Miocene ice sheet dynamics, deep-sea temperatures, and carbon cycling: A Southern Ocean perspective. *Geochemistry, Geophysics, Geosystems*, 9, Q02006. https://doi.org/10.1029/2007GC001736
- Stein, R., Fahl, K., Schreck, M., Knorr, G., Niessen, F., Forwick, M., et al. (2016). Evidence for ice-free summers in the late Miocene Central Arctic Ocean. *Nature Communications*, 7(1), 11148. https://doi.org/10.1038/ncomms11148
- Super, J. R., Thomas, E., Pagani, M., Huber, M., O'Brien, C., & Hull, P. M. (2018). North Atlantic temperature and pCO₂ coupling in the early-middle Miocene. *Geology*, 46(6), 519–522. https://doi.org/10.1130/G40228.1
- Tierney, J. E., & Tingley, M. P. (2018). BAYSPLINE: A new calibration for the alkenone paleothermometer. *Paleoceanography and Paleoclimatology*, 33, 281–301. https://doi.org/10.1002/2017PA003201
- Utescher, T., Ashraf, A. R., Dreist, A., Dybkjær, K., Mosbrugger, V., Pross, J., & Wilde, V. (2012). Variability of Neogene continental climates in Northwest Europe—A detailed study based on microfloras. *Turkish Journal of Earth Sciences*, 21(2), 289–314.
- Utescher, T., Bohme, M., & Mosbrugger, V. (2011). The Neogene of Eurasia: Spatial gradients and temporal trends—The second synthesis of NECLIME. *Palaeogeography, Palaeoclimatology, Palaeoecology*, 304(3–4), 196–201. https://doi.org/10.1016/j.palaeo.2011.03.012
- Utescher, T., Dreist, A., Henrot, A.-J., Hickler, T., Liu, Y.-S., Mosbrugger, V., et al. (2017). Continental climate gradients in North America and Western Eurasia before and after the closure of the central American seaway. *Earth and Planetary Science Letters*, 472, 120–130. https://doi.org/10.1016/j.epsl.2017.05.019
- Utescher, T., Mosbrugger, V., Ivanov, D., & Dilcher, D. L. (2009). Present-day climatic equivalents of European Cenozoic climates. Earth and Planetary Science Letters, 284(3-4), 544-552. https://doi.org/10.1016/j.epsl.2009.05.021
- Wang, L., Longo, W. M., Dillon, J. T., Zhao, J., Zheng, Y., Moros, M., & Huang, Y. (2019). An efficient approach to eliminate steryl ethers and miscellaneous esters/ketones for gas chromatographic analysis of alkenones and alkenoates. *Journal of Chromatography A*, 1596, 175–182. https://doi.org/10.1016/j.chroma.2019.02.064
- Warny, S., & Askin, R. (2011). Last remnants of Cenozoic vegetation and organic-walled phytoplankton in the Antarctic Peninsula's ice-house world. In *Tectonic, climatic, and cryospheric evolution of the Antarctic peninsula* (Vol. 63, pp. 167–192). Washington, DC: American Geophysical Union.
- Warny, S., Askin, R. A., Hannah, M. J., Mohr, B. A., Raine, J. I., Harwood, D. M., Florindo, F., & the SMS Science Team (2009). Palynomorphs from a sediment core reveal a sudden remarkably warm Antarctica during the middle Miocene. *Geology*, 37(10), 955–958. https://doi.org/10.1130/G30139A.1
- You, Y., Huber, M., Müller, R., Poulsen, C., & Ribbe, J. (2009). Simulation of the middle Miocene climate optimum. *Geophysical Research Letters*, 36, L04702. https://doi.org/10.1029/2008GL036571
- Zachos, J., Pagani, M., Sloan, L., Thomas, E., & Billups, K. (2001). Trends, rhythms, and aberrations in global climate 65 Ma to present. Science, 292, 686–693.
- Zhang, Y. G., Pagani, M., & Liu, Z. (2014). A 12-million-year temperature history of the tropical Pacific Ocean. *Science*, 344(6179), 84–87. https://doi.org/10.1126/science.1246172
- Zhang, Y. G., Pagani, M., Liu, Z., Bohaty, S. M., & DeConto, R. (2013). A 40-million-year history of atmospheric CO₂. Philosophical Transactions of the Royal Society A Mathematical Physical and Engineering Sciences, 371(2001), 20130096.
- Ziegler, P. A. (1990). Geological atlas of western and central Europe (pp. 1–239). Bath: Geological Society.

HERBERT ET AL. 10 of 10